Scattering from Dielectric Structures Above Impedance Surfaces and Resistive Sheets

Kamal Sarabandi

Abstract—**Interest in understanding of electromagnetic interaction with rough surfaces has prompted the study of scattering from typical dielectric humps over impedance surfaces. It is shown that the Green's function of the problem for a resistive sheet resembles that of the impedance surface. Hence both problems are considered here. In this paper a numerical solution for the scattered field of a two-dimensional dielectric object, possibly inhomogeneous, with arbitrary cross section above the impedance surface or resistive sheet is sought. First the Green's function of the problem is derived based on the exact image theory. This form of the Green's function is amenable to numerical computation. Then the induced polarization currents are calculated by casting the integral equations into a matrix equation via the method of moments. Numerical problems in calculation of the Green's function when both source and observation points are close to the surface are discussed. Comparison of numerical results for both transverse electric (TE) and transverse magnetic (TM) cases with a perturbation solution shows excellent agreement between the two methods.**

I. Introduction

APPLICATION of electromagnetic waves as a means of retrieving the desired surface parameters of the earth is a matter of increasing concern. For example, soil moisture content and surface roughness are two such parameters. The problem of electromagnetic wave scattering by rough surfaces has long been studied and because of its complexity satisfactory models exist only for a limited cases. The existing models are applicable to two extreme roughness conditions. In the so-called small perturbation model both the correlation length and root mean square (rms) height must be smaller than a wavelength [1]. For the other extreme, known as the Kirchoff model, however, both the correlation length and rms height must be much larger than a wavelength while the rms slope must be reasonably small [1]. To achieve analytical expressions for the scattering coefficients, the random surface medium is assumed to be homogeneous and to have a Gaussian autocorrelation function.

Measurement of natural surfaces at microwave frequencies shows that the existing models are inadequate to explain the scattering behavior for two main reasons [2]. First, the roughness parameters are usually outside the region of validity of the mentioned models. Second, natural surfaces are not homogeneous, that is the moisture content in most cases is not uniform in depth. The top rough layer includes clods and rocks that are usually dry and keep the moisture of the underlying layer from evaporating. The moist smooth underlying soil layer at microwave frequencies can be modeled by an impedance surface and irregularities at the top by dielectric humps of different dielectric constants. To simulate the electromagnetic scattering behavior of such surfaces, the scattering solution of an isolated hump is needed.

In this paper we seek a numerical solution of a two-dimensional dielectric object with arbitrary cross section above a uniform impedance surface when the object is illuminated by a plane wave. The geometry of the problem is depicted in Fig. 1. Common practice in obtaining the Green's function for scattering and antenna problems in the presence of a half-space medium is through calculation of a Sommerfeld-type integral [3]. These infinite integrals, in general, are highly oscillatory and computationally rather inefficient. Although many techniques have been developed to speed up their calculation for three-dimensional problems [4], [5] they are of little use for two-dimensional problems. Numerical solutions for two-dimensional scattering problems in the presence of a half-space medium have been limited to small scatterers or low frequencies mainly because of difficulties in computing the Green's function [6], [7]. Here, the Green's function of an impedance surface (or resistive sheet) is derived in terms of rapidly converging integrals using appropriate integral transforms. Useful asymptotic expressions of the Green's function are also given. The scattering problem is then formulated by integral equations which are solved numerically using the method of moments.

II. Derivation of Green's Function Using Exact Image Theory

The first step toward calculating the scattered field of an object is to derive the dyadic Green's function of the problem. Since the Green's function is used in a numerical solution of the scattering problem, it should be efficiently calculable. An integral representation for the image of a line source above an impedance surface or a resistive sheet is derived using integral transforms similar to those employed by Lindell and Alanen in derivation of the exact image theory [8]. Interested readers are also referred to [9]–[11] for detailed discussion of the exact image theory. The new representation for the Green's function has an excellent rate of convergence for most practical purposes and can be computed very easily.

The fields generated by a two-dimensional ($\partial/\partial z = 0$) distribution of electric current ($\mathbf{J}_e(x, y)$) in terms of the

Manuscript received March 26, 1991; revised October 3, 1991. This work was supported by NASA under Contract NAGW-2151.

The author is with the Radiation Laboratory, Department of Electrical Engineering and Computer Science, University of Michigan, Ann Arbor, MI 48109-2122.

IEEE Log Number 9105277.

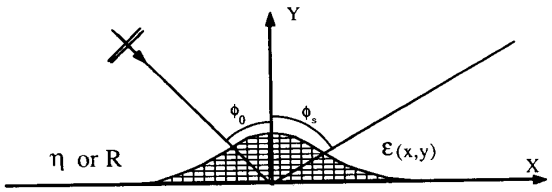

Impedance Surface or Resistive Sheet

Fig. 1. Geometry for the scattering problem of a dielectric cylinder above a uniform resistive or impedance sheet.

associated Hertz vector potential are given by

$$E_x = k_0^2\left(1 + \frac{1}{k_0^2}\frac{\partial^2}{\partial x^2}\right)\Pi_x + \frac{\partial^2}{\partial x\,\partial y}\Pi_y,$$

$$E_y = \frac{\partial^2}{\partial y\,\partial x}\Pi_x + k_0^2\left(1 + \frac{1}{k_0^2}\frac{\partial^2}{\partial y^2}\right)\Pi_y, \qquad (1)$$

$$E_z = k_0^2\Pi_z.$$

The Hertz vector potential associated with an infinite current filament located at point (x', y') in free space with amplitude I_p and orientation $\hat{p}$ is of the form

$$\Pi_p(x, y) = \frac{-Z_0}{4k_0}H_0^{(1)}\left(k_0\sqrt{(x-x')^2 + (y-y')^2}\right)I_p, \qquad p = x,\ y \text{ or } z \quad (2)$$

where $H_0^{(1)}$ is the Hankel function of the first kind and zeroth order and Z_0 is the free space characteristic impedance. The corresponding field components can be obtained by inserting (2) into (1) and then by employing the identity

$$H_0^{(1)}\left(k_0\sqrt{(x-x')^2 + (y-y')^2}\right) = \frac{1}{\pi}\int_{-\infty}^{+\infty}\frac{e^{ik_y|y-y'| - ik_x(x-x')}}{k_y}\,dk_x \quad (3)$$

the resulting fields can be expressed in terms of a continuous spectrum of plane waves. In (3) $k_y = \sqrt{k_0^2 - k_x^2}$ and the branch of the square root is chosen such that $\sqrt{-1} = i$.

In the presence of the impedance surface or the resistive sheet, when the current filament is in the upper half-space, each plane wave is reflected at the interface according to the appropriate reflection coefficient. It should be noted that the incidence angle of each plane wave, in general, is complex and is given by $\gamma = \arctan(k_x/k_y)$. The net effect of the impedance surface or resistive sheet on the radiated field can be obtained by superimposing all of the reflected plane waves of the form $R_q(\gamma)e^{ik_y(y+y')-ik_x(x-x')}$, where $R_q(\gamma)$ is the reflection coefficient corresponding to incident polarization $q = E$ or H and the surface type. The total reflected field can now be obtained by noting that

$$E_x^r = -R_H(\gamma)E_x^i, \quad E_y^r = R_H(\gamma)E_y^i, \quad E_z^r = R_E(\gamma)E_z^i$$

and since the direction of propagation along the y axis is reversed for the reflected waves, the operator $\partial/\partial y$ for the x and y components of the reflected field must be replaced with $-\partial/\partial y$. Thus, in matrix notation the total field in the upper half-space can be represented by

$$\mathbf{E} = \begin{bmatrix} G_{xx} & G_{xy} & 0 \\ G_{yx} & G_{yy} & 0 \\ 0 & 0 & G_{zz} \end{bmatrix}\begin{bmatrix} I_x \\ I_y \\ I_z \end{bmatrix} \qquad (4)$$

where

$$G_{xx} = -\frac{k_0Z_0}{4}\left(1 + \frac{1}{k_0^2}\frac{\partial^2}{\partial x^2}\right)\cdot\left[H_0^{(1)}\left(k_0\sqrt{(x-x')^2 + (y-y')^2}\right) - Q_H\right]$$

$$G_{xy} = -\frac{Z_0}{4k_0}\frac{\partial^2}{\partial x\,\partial y}\cdot\left[H_0^{(1)}\left(k_0\sqrt{(x-x')^2 + (y-y')^2}\right) + Q_H\right]$$

$$G_{yx} = -\frac{Z_0}{4k_0}\frac{\partial^2}{\partial y\,\partial x}\cdot\left[H_0^{(1)}\left(k_0\sqrt{(x-x')^2 + (y-y')^2}\right) - Q_H\right]$$

$$G_{yy} = -\frac{k_0Z_0}{4}\left(1 + \frac{1}{k_0^2}\frac{\partial^2}{\partial y^2}\right)\cdot\left[H_0^{(1)}\left(k_0\sqrt{(x-x')^2 + (y-y')^2}\right) + Q_H\right]$$

$$G_{zz} = -\frac{k_0Z_0}{4}\cdot\left[H_0^{(1)}\left(k_0\sqrt{(x-x')^2 + (y-y')^2}\right) + Q_E\right] \quad (5)$$

are the elements of the dyadic Green's function ($\mathbf{G}(x, y; x', y')$) for the two-dimensional impedance surface or resistive sheet problem. In (5) the quantity $Q_{\substack{H\\E}}$ is given by

$$Q_{\substack{H\\E}}(x, y; x', y') = \frac{1}{\pi}\int_{-\infty}^{+\infty}R_{\substack{H\\E}}(\gamma)\cdot\frac{e^{ik_y(y+y')-ik_x(x-x')}}{k_y}\,dk_x \quad (6)$$

and the expressions for the reflection coefficients of the impedance surface and resistive sheet are respectively given by [12]

$$R_E(\gamma) = \frac{\eta\cos\gamma - 1}{\eta\cos\gamma + 1} \qquad R_H(\gamma) = \frac{\cos\gamma - \eta}{\cos\gamma + \eta} \quad (7)$$

$$R_E(\gamma) = \frac{-1}{1 + 2R\cos\gamma} \qquad R_H(\gamma) = \frac{1}{1 + 2R\sec\gamma} \quad (8)$$

where η is the normalized impedance of the impedance surface ($\eta = Z/Z_0$) and R is the normalized resistivity of

the resistive sheet. For example the resistivity of an infinitesimally thin dielectric layer of thickness τ and permittivity ϵ is given by [13]

$$R = \frac{i}{k_0 \tau(\epsilon - 1)}.$$

If an electric current distribution $\mathbf{J}_e$ occupies region S in the upper half-space, the radiated electric field at any point in the upper half-space can be obtained from:

$$\mathbf{E}^s(x, y) = \int_S \mathbf{G}(x, y; x', y') \cdot \mathbf{J}(x', y')\, dx'\, dy'. \quad (9)$$

The first term within brackets in (5) represents the effect of the current filament in the absence of the impedance surface while the second term is due to the image of the current filament. Unfortunately, the integral representing the contribution of the image does not have a closed form and its convergence rate is very poor. To achieve the image contribution in an efficient way consider the following transformation:

$$\int_0^{+\infty} e^{-\alpha v} e^{-k_y v}\, dv = \frac{1}{\alpha + k_y},$$

$$\text{provided } \mathrm{Re}[\alpha] > -\mathrm{Re}[k_y]. \quad (10)$$

The choice of the branch cut for k_y guarantees that $\mathrm{Re}[k_y]$ is nonnegative as k_x takes any real number, therefore the sufficient condition for (10) is

$$\mathrm{Re}[\alpha] > 0.$$

The expressions for the reflection coefficients can be written in terms of k_y by substituting $\cos\gamma = k_y/k_0$. For the case of a resistive sheet with an E-polarized incident wave we can define α to be $k_0/2R$, noting that the above condition is satisfied ($\mathrm{Re}[\alpha] = k_0^2 \tau \epsilon''/2 > 0$). In view of the transformation (10) the integral representing the image contribution in the upper half-space can be written as

$$\int_{-\infty}^{+\infty} \frac{-1}{\left(1 + \frac{k_y}{\alpha}\right) k_y} e^{ik_y(y+y') - ik_x(x-x')}\, dk_x$$

$$= \int_0^{+\infty} -\alpha e^{-\alpha v} \left[\int_{-\infty}^{+\infty} \frac{e^{ik_y(y+y'+iv) - ik_x(x-x')}}{k_y}\, dk_x \right] dv.$$

Employing the identity given by (3), the zz-component of the dyadic Green's function for the resistive sheet problem in the upper half-space can be obtained from

$$G_{zz}^{+} = \frac{-k_0 Z_0}{4} \left[H_0^{(1)}\left(k_0 \sqrt{(x-x')^2 + (y-y')^2}\right) - \int_0^{+\infty} \alpha e^{-\alpha v} \cdot H_0^{(1)}\left(k_0 \sqrt{(x-x')^2 + (y+y'+iv)^2}\right) dv \right]. \quad (11)$$

In a similar manner for the lower half-space the zz-component becomes

$$G_{zz}^{-} = \frac{-k_0 Z_0}{4} \left[H_0^{(1)}\left(k_0 \sqrt{(x-x')^2 + (-y+y')^2}\right) - \int_0^{+\infty} \alpha e^{-\alpha v} \cdot H_0^{(1)}\left(k_0 \sqrt{(x-x')^2 + (-y+y'+iv)^2}\right) dv \right]. \quad (12)$$

This integral representation converges very fast because both functions in the integrand are exponentially decaying. Also from this representation it can be deduced that the image of a line current above a resistive sheet is a half-plane current with exponential distribution and is located in the complex y-plane occupying the region $-y' - i\infty < y < -y'$ (see Fig. 2).

Similarly by defining $\beta = 2Rk_0$ for the case of H-polarization the quantity Q_H in (6) for a resistive sheet in the upper half-space is given by

$$Q_H = H_0^{(1)}\left(k_0 \sqrt{(x-x')^2 + (y+y')^2}\right) - \int_0^{+\infty} \beta e^{-\beta v} \cdot H_0^{(1)}\left(k_0 \sqrt{(x-x')^2 + (y+y'+iv)^2}\right) dv. \quad (13)$$

In the corresponding case of an impedance surface the dyadic Green's function can be obtained from (5) with the following expressions for the quantities Q_E and Q_H

$$Q_E = H_0^{(1)}\left(k_0 \sqrt{(x-x')^2 + (y+y')^2}\right) - 2\int_0^{+\infty} \alpha' e^{-\alpha' v} \cdot H_0^{(1)}\left(k_0 \sqrt{(x-x')^2 + (y+y'+iv)^2}\right) dv \quad (14)$$

$$Q_H = H_0^{(1)}\left(k_0 \sqrt{(x-x')^2 + (y+y')^2}\right) - 2\int_0^{+\infty} \beta' e^{-\beta' v} \cdot H_0^{(1)}\left(k_0 \sqrt{(x-x')^2 + (y+y'+iv)^2}\right) dv. \quad (15)$$

The quantities α' and β' in (14) and (15) in terms of the normalized surface impedance are, respectively, given by

$$\alpha' = \frac{k_0}{\eta}, \quad \beta' = k_0 \eta.$$

The validity of the new image representation can be checked by considering some special limiting cases. For example consider the resistive sheet problem for E-polarization. Suppose the resistivity is very small (approaching perfect conductivity) which implies that $|\alpha| \gg 1$. In this case contribution to the integral in (11) comes mostly from point $v = 0$

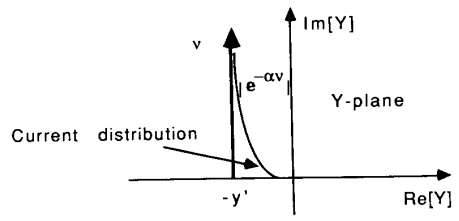

Fig. 2. The location of the image of the line source in the complex Y plane.

and therefore

$$\int_0^{+\infty} \alpha e^{-\alpha v} H_0^{(1)}\left(k_0\sqrt{(x-x')^2+(y+y'+iv)^2}\right) dv$$
$$\approx H_0^{(1)}\left(k_0\sqrt{(x-x')^2+(y+y')^2}\right)\int_0^{+\infty} \alpha e^{-\alpha v}\, dv$$
$$= H_0^{(1)}\left(k_0\sqrt{(x-x')^2+(y+y')^2}\right)$$

which is the image for the perfectly conducting case. The asymptotic behavior of the integral in terms of a convergent series of inverse power of α can also be obtained by performing integration by parts repeatedly, that is

$$\int_0^{+\infty} \alpha e^{-\alpha v} H_0^{(1)}\left(k_0\sqrt{(x-x')^2+(y+y'+iv)^2}\right) dv = \sum_{n=0}^{\infty}\left(\frac{-1}{\alpha}\right)^n h^{(n)}(0) \quad (16)$$

where $h^{(n)}(0)$ is the nth derivative of $H_0^{(1)}(k_0\sqrt{(x-x')^2+(y+y'+iv)^2})$ with respect to v evaluated at zero. The first order of approximation is

$$\sum_{n=0}^{\infty}\left(\frac{-1}{\alpha}\right)^n h^{(n)}(0) \approx h(0) - h'(0)\frac{1}{\alpha} \approx h\left(\frac{-1}{\alpha}\right)$$
$$= H_0^{(1)}\left(k_0\sqrt{(x-x')^2+\left(y+y'-\frac{i}{\alpha}\right)^2}\right)$$

which is a line image located in the complex plane at $y = -y' + i/\alpha$. As it is important in the scattering problems, the other asymptotic behavior of interest is the far field approximation where the point of observation is far from the image point, i.e., $\rho_2 = \sqrt{(x-x')^2+(y+y')^2} \gg \lambda_0$. In this condition

$$\sqrt{(x-x')^2+(y+y'+iv)^2} \approx \rho_2\left(1+\frac{iv\cos\phi_2}{\rho_2}\right)$$

where we have assumed that $\rho_2 \gg v$. The validity of this assumption comes from the fact that the integrand of (16) is approximately zero if $v > v_{\max}$ for some finite $v_{\max}$. Now by using the large argument expansion of the Hankel function and then substituting for α we get

$$\lim_{\rho_2\to\infty}\int_0^{+\infty} -\alpha e^{-\alpha v} \cdot H_0^{(1)}\left(k_0\sqrt{(x-x')^2+(y+y'+iv)^2}\right) dv$$
$$\approx \sqrt{\frac{2}{\pi k_0\rho_2}}\, e^{i(k_0\rho_2-\pi/4)}\frac{-1}{1+2R\cos\phi}.$$

Note that the last term in the above equation is the plane wave reflection coefficient for the E-polarization case. This result is identical to the asymptotic value of the integral given by (6) evaluated using the saddle point technique. In applying the saddle point technique the poles associated with the reflection coefficient function ($R_q(\gamma)$) may be captured when the contour is deformed. The contribution of these poles gives rise to surface waves, but their effect can be ignored if the surface is lossy and the observation point is away from the interface. Also, the large-argument expansion of the Hankel function can be used for the distant approximation. Now it can easily be shown that for an electric current distribution $\mathbf{J}_e$, the radiated far field does not have a $\hat{\rho}$ component and the far-field amplitude defined by

$$\mathbf{E} = \sqrt{\frac{2}{\pi k_0\rho}}\, e^{i(k_0\rho-\pi/4)}\mathbf{S}$$

has the following components:

$$S_\phi = \frac{k_0 Z_0}{4}\left\{\int_S \cos\phi J_x(x',y') \cdot e^{-ik_0\sin\phi x'}\left[e^{-ik_0\cos\phi y'} - R_H(\phi)e^{ik_0\cos\phi y'}\right] dx'\,dy' - \int_S \sin\phi J_y(x',y') \cdot e^{-ik_0\sin\phi x'}\left[e^{-ik_0\cos\phi y'} + R_H(\phi)e^{ik_0\cos\phi y'}\right] dx'\,dy'\right\} \quad (17)$$

$$S_z = -\frac{k_0 Z_0}{4}\int_S J_z(x',y') \cdot e^{-ik_0\sin\phi x'}\left[e^{-ik_0\cos\phi y'} + R_E(\phi)e^{ik_0\cos\phi y'}\right] dx'\,dy'.$$

III. Derivation of Integral Equations

Suppose a dielectric object, possibly inhomogeneous, is located above an impedance surface (resistive sheet) and is illuminated by a plane wave. The direction of propagation of the plane wave is denoted by the angle ϕ_0 measured from the normal to the surface. Therefore the incident wave for E- and H-polarization cases may be represented by

$$\mathbf{E}^i = \hat{z}e^{ik_0(\sin\phi_0 x - \cos\phi_0 y)},$$
$$\mathbf{E}^i = (\cos\phi_0\hat{x} + \sin\phi_0\hat{y})e^{ik_0(\sin\phi_0 x - \cos\phi_0 y)}.$$

The incident field induces conduction and displacement currents in the dielectric object which together are known as the polarization current. The polarization current in terms of the

total electric field ($\mathbf{E}^t$) inside the dielectric object is given by

$$\mathbf{J}_e = -ik_0 Y_0(\epsilon(x, y) - 1)\mathbf{E}^t \tag{18}$$

where $\epsilon(x, y)$ represents the relative dielectric constant of the object. The total field is comprised of the incident, reflected, and scattered fields which are, respectively, denoted by $\mathbf{E}^i$, $\mathbf{E}^r$, and $\mathbf{E}^s$, then

$$\mathbf{E}^t = \mathbf{E}^i + \mathbf{E}^r + \mathbf{E}^s. \tag{19}$$

In the E-polarization case where the electric field is perpendicular to the plane of incidence the incident field excites a z-directed polarization current, which leads to a scattered field in the z direction. For the H-polarization case, however, the polarization current and the scattered field are in the transverse plane and therefore the integral equations for E- and H-polarization cases are decoupled. Using (9) for the scattered field and (19) for the total field with (18) the following integral equations for the polarization currents can be derived

$$\begin{aligned} J_z(x, y) = -ik_0 Y_0(\epsilon(x, y) - 1)\Big\{ & e^{ik_0 \sin\phi_0 x} \\ & \cdot \left(e^{-ik_0 \cos\phi_0 y} + R_E(\phi_0) e^{ik_0 \cos\phi_0 y}\right) \\ & + \int\int_s J_z(x', y') G_{zz}(x, y; x', y')\, dx'\, dy' \Big\}. \end{aligned} \tag{20}$$

$$\begin{aligned} J_x(x, y) = -ik_0 Y_0(\epsilon(x, y) - 1)\Big\{ & \cos\phi_0 e^{ik_0 \sin\phi_0 x} \\ & \cdot \left(e^{-ik_0 \cos\phi_0 y} - R_H(\phi_0) e^{ik_0 \cos\phi_0 y}\right) \\ & + \int\int_s \left[J_x(x', y') G_{xx}(x, y; x', y') \right. \\ & \left. + J_y(x', y') G_{xy}(x, y; x', y') \right] dx'\, dy' \Big\} \end{aligned} \tag{21}$$

$$\begin{aligned} J_y(x, y) = -ik_0 Y_0(\epsilon(x, y) - 1)\Big\{ & \sin\phi_0 e^{ik_0 \sin\phi_0 x} \\ & \cdot \left(e^{-ik_0 \cos\phi_0 y} + R_H(\phi_0) e^{ik_0 \cos\phi_0 y}\right) \\ & + \int\int_s \left[J_x(x', y') G_{yx}(x, y; x', y') \right. \\ & \left. + J_y(x', y') G_{yy}(x, y; x', y') \right] dx'\, dy' \Big\}. \end{aligned} \tag{22}$$

IV. The Method of Moments Solution

There is no known exact solution for the integral equations that were developed in the previous section. In this section an approximate numerical solution of these equations is obtained by employing the method of moments.

Let us divide the cross section of the dielectric structure into N sufficiently small rectangular cells such that the dielectric constant and the polarization current can be approximated by constant values over each cell. First consider the integral equation (20), which corresponds to the E-polarization case. Using the point matching technique the integral equation can be cast into a matrix equation of the following form:

$$[\mathscr{Z}][\mathscr{J}] = [\mathscr{V}] \tag{23}$$

where $[\mathscr{Z}]$ is the impedance matrix, $[\mathscr{J}]$ is the unknown vector whose entries are the value of polarization current at the center of each cell, i.e., (x_n, y_n), and finally $[\mathscr{V}]$ is the excitation vector whose entries are given by

$$\begin{aligned} v_n = {} & ik_0 Y_0(\epsilon(x_n, y_n) - 1) \\ & \cdot e^{ik_0 \sin\phi_0 x_n}\left(e^{-ik_0 \cos\phi_0 y_n} + R_E(\phi_0) e^{ik_0 \cos\phi_0 y_n}\right). \end{aligned}$$

The off-diagonal elements of the impedance matrix can be obtained by approximating the Green's function via its Taylor series expansion around the midpoint of each cell and then performing the integration analytically. This technique allows us to choose very small cell sizes without incurring too much error because of the adjacent cells. For diagonal elements the free space Green's function is approximated by its small argument expansion and then integration is performed analytically over the cell area. This allows us to choose rectangular shape cells instead of squares that are approximated by circles of equal areas in the traditional method [14]. In order to give the expressions for elements of the impedance matrix, let us define the following functions

$$\begin{aligned} U_{mn}^q = {} & -H_0^{(1)}(k_0 r_{mn}^q)\cos^2\theta_{mn}^q \\ & + \frac{H_1^{(1)}(k_0 r_{mn}^q)}{k_0 r_{mn}^q}\left(\cos^2\theta_{mn}^q - \sin^2\theta_{mn}^q\right) \end{aligned} \tag{24}$$

$$\begin{aligned} V_{mn}^q = {} & -H_0^{(1)}(k_0 r_{mn}^q)\sin^2\theta_{mn}^q \\ & + \frac{H_1^{(1)}(k_0 r_{mn}^q)}{k_0 r_{mn}^q}\left(\sin^2\theta_{mn}^q - \cos^2\theta_{mn}^q\right) \end{aligned} \tag{25}$$

where r_{mn}^q and θ_{mn}^q are the distance and the angle from the source, its mirror image, and its continuous image points to the observation point which are given by

$$r_{mn}^q = \begin{cases} \sqrt{(x_m - x_n)^2 + (y_m - y_n)^2}, & \text{if } q = s \\ \sqrt{(x_m - x_n)^2 + (y_m + y_n)^2}, & \text{if } q = i \\ \sqrt{(x_m - x_n)^2 + (y_m + y_n + iv)^2}, & \text{if } q = c \end{cases}$$

$$\theta_{mn}^q = \begin{cases} \arctan\left(\dfrac{y_m - y_n}{x_m - x_n}\right), & \text{if } q = s \\ \arctan\left(\dfrac{y_m + y_n}{x_m - x_n}\right), & \text{if } q = i \\ \arctan\left(\dfrac{y_m + y_n + iv}{x_m - x_n}\right), & \text{if } q = c. \end{cases}$$

The diagonal entries of the impedance matrix for resistive

sheet are given by

$$z_{nn} = -1 - \frac{1}{\pi}(\epsilon(x_n, y_n) - 1)\left\{\frac{k_0^2 \Delta x_n \Delta y_n}{2} \cdot \left[\ln\left(\frac{k_0}{4}\sqrt{\Delta x_n^2 + \Delta y_n^2}\right) + \gamma - \frac{i\pi}{2} - \frac{3}{2}\right] + \left(\frac{k_0 \Delta x_n}{2}\right)^2 \arctan\left(\frac{\Delta y_n}{\Delta x_n}\right) + \left(\frac{k_0 \Delta y_n}{2}\right)^2 \left(\frac{\pi}{2} - \arctan\left(\frac{\Delta y_n}{\Delta x_n}\right)\right)\right\} - \frac{ik_0^2 \Delta x_n \Delta y_n}{4}(\epsilon(x_n, y_n) - 1)\alpha \cdot \int_0^\infty e^{-\alpha\nu} H_0^{(1)}(k_0 r_{nn}^c)\, d\nu \quad (26)$$

and the nondiagonal entries are expressed by

$$z_{mn} = \frac{ik_0^2 \Delta x_n \Delta y_n}{4}(\epsilon(x_m, y_m) - 1)\left\{H_0^{(1)}(k_0 r_{mn}^s) + \frac{(k_0 \Delta x_n)^2}{24} U_{mn}^s + \frac{(k_0 \Delta y_n)^2}{24} V_{mn}^s - \alpha \int_0^\infty e^{-\alpha\nu} H_0^{(1)}(k_0 r_{mn}^c)\, d\nu\right\}. \quad (27)$$

Here, Δx_n and Δy_n are the dimensions of the nth rectangular cell and $\gamma = 0.57721$ is Euler's constant. The entries of the impedance matrix for the impedance surface can also be obtained in asimilar fashion by adding the mirror contribution, replacing α with α' and doubling the integrals in (26) and (27).

The integrals in (26) and (27) are evaluated numerically using the Gauss-Legendre quadrature technique [15]. It should be mentioned here that when the observation and source points are both close to the surface ($k_0(y_m + y_n) \ll 1$) for some value of $\nu = \nu_0$, the distance function $r_0 = \sqrt{(x_m - x_n)^2 + (y_m + y_n + i\nu_0)^2}$ becomes very small. Consequently the integrand of the integral representing the image contribution varies very rapidly around this point. In order to evaluate the integral accurately, the contribution of the integrand around ν_0 should be evaluated analytically. The integrand achieves its maximum when the absolute value of the distance function is minimum. This minimum occurs at

$$\nu_0 = \sqrt{(x_m - x_n)^2 - (y_m + y_n)^2}. \quad (28)$$

If the argument of the square root in (28) is negative, then the distance function takes its minimum at $\nu_0 = 0$. Fig. 3 shows the integrand function in (27) when both observation and source points are very close to the surface. The analytical evaluation of the integral around the point ν_0 can be performed by using the small argument expansion of the Hankel

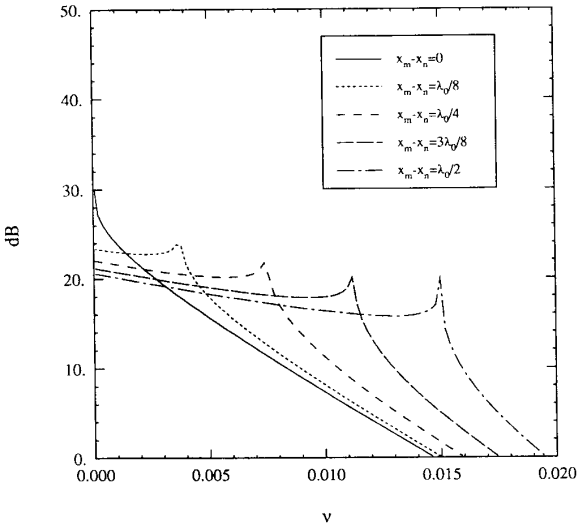

Fig. 34. The absolute value of the integrand function in (30) for $R = 0.18 + i0.37$ at 10 GHz, $y_m + y_n = 6 \times 10^{-5}\ \lambda_0$, and five values of $x_m - x_n$.

function, i.e.,

$$\int_{\nu_0 - \Delta\nu}^{\nu_0 + \Delta\nu} e^{-\alpha\nu} H_0^{(1)}(k_0 r_{mn}^c)\, d\nu = e^{-\alpha\nu_0}\left[2\,\Delta\nu\left(1 + \frac{i2\gamma}{\pi}\right) + \frac{i2}{\pi} I_1\right]$$

where

$$I_1 = \frac{i}{2}(y_m + y_n + i\nu_0) \cdot \ln\frac{r_0^2 - \Delta\nu^2 - i2\,\Delta\nu(y_m + y_n + i\nu_0)}{r_0^2 - \Delta\nu^2 + i2\,\Delta\nu(y_m + y_n + i\nu_0)} + \frac{x_m - x_n}{2}\ln\frac{r_0^2 + \Delta\nu^2 + 2\,\Delta\nu(x_m - x_n)}{r_0^2 + \Delta\nu^2 - 2\,\Delta\nu(x_m - x_n)} - \Delta\nu\left[2 - \ln\frac{k_0^2}{4} \cdot \sqrt{(r_0^2 - \Delta\nu^2)^2 + 4\,\Delta\nu^2(y_m + y_n + i\nu_0)^2}\right].$$

For self-cell (diagonal element) calculation we note that $x_m = x_n$, which renders $\nu_0 = 0$ and

$$\int_0^{\Delta\nu} e^{-\alpha\nu} H_0^{(1)}(k_0 r_{mn}^c)\, d\nu = \Delta\nu\left(1 + \frac{i2\gamma}{\pi}\right) + \frac{2}{\pi} I_1'$$

where

$$I_1' = (y_m + y_n)\ln\frac{y_m + y_n + i\,\Delta\nu}{y_m + y_n} + i\,\Delta\nu\left[\ln\frac{k_0(y_m + y_n + i\,\Delta\nu)}{2} - 1\right].$$

In the H-polarization case, using the same partitioning of the cross section of the dielectric body, the coupled integral

equations (21) and (22) can be cast into a matrix equation similar to (23) where

$$[\mathcal{J}] = \begin{bmatrix} \mathcal{J}_x \\ \mathcal{J}_y \end{bmatrix}, \quad [\mathcal{Z}] = \begin{bmatrix} \mathcal{Z}_1 & \mathcal{Z}_2 \\ \mathcal{Z}_3 & \mathcal{Z}_4 \end{bmatrix}, \quad \text{and}$$

$$[\mathcal{V}] = \begin{bmatrix} \mathcal{V}_x \\ \mathcal{V}_y \end{bmatrix}.$$

The elements of the excitation vector are given by ($n = 1, \cdots, N$)

$$v_n = ik_0 Y_0 (\epsilon(x_n, y_n) - 1) \cos\phi_0 \cdot e^{ik_0 \sin\phi_0 x_n} \left(e^{-ik_0 \cos\phi_0 y_n} - R_H(\phi_0) e^{ik_0 \cos\phi_0 y_n}\right)$$

$$v_{n+N} = ik_0 Y_0 (\epsilon(x_n, y_n) - 1) \sin\phi_0 \cdot e^{ik_0 \sin\phi_0 x_n} \left(e^{-ik_0 \cos\phi_0 y_n} + R_H(\phi_0) e^{ik_0 \cos\phi_0 z_m}\right).$$

Here again the entries of the impedance matrix are obtained by expansion of the Green's function over each cell as explained in the E-polarization case. Since the Green's function has a higher degree of singularity in this case, these expansions are even more important to use in order to avoid anomalous errors.

For the resistive sheet the nondiagonal elements of the impedance matrix are given by

$$z_{1mn} = \frac{ik_0^2 \Delta x_n \Delta y_n}{4} (\epsilon(x_m, y_m) - 1) \cdot \left\{ A^s_{mn} - A^i_{mn} + \beta \int_0^\infty e^{-\beta\nu} A^c_{mn}\, d\nu \right\} \quad (29)$$

$$z_{2mn} = \frac{ik_0^2 \Delta x_n \Delta y_n}{4} (\epsilon(x_m, y_m) - 1) \cdot \left\{ B^s_{mn} + B^i_{mn} - \beta \int_0^\infty e^{-\beta\nu} B^c_{mn}\, d\nu \right\} \quad (30)$$

$$z_{3mn} = \frac{ik_0^2 \Delta x_n \Delta y_n}{4} (\epsilon(x_m, y_m) - 1) \cdot \left\{ B^s_{mn} - B^i_{mn} + \beta \int_0^\infty e^{-\beta\nu} B^c_{mn}\, d\nu \right\} \quad (31)$$

$$z_{4mn} = \frac{ik_0^2 \Delta x_n \Delta y_n}{4} (\epsilon(x_m, y_m) - 1) \cdot \left\{ C^s_{mn} + C^i_{mn} - \beta \int_0^\infty e^{-\beta\nu} C^c_{mn}\, d\nu \right\} \quad (32)$$

where A^q_{mn}, B^q_{mn}, and C^q_{mn} are given in the Appendix. Noting that $\cos\theta^i_{nn} = \cos\theta^c_{nn} = 0$ and $\sin\theta^i_{nn} = \sin\theta^c_{nn} = 1$, the diagonal elements are of the following form:

$$z_{1nn} = -1 - \frac{1}{\pi}(\epsilon(x_n, y_n) - 1) \left\{ \frac{k_0^2 \Delta x_n \Delta y_n}{4} \cdot \left[\ln\left(\frac{k_0}{4} \sqrt{\Delta x_n^2 + \Delta y_n^2} \right) + \gamma - \frac{i\pi}{2} - \frac{3}{2} \right] + 2 \arctan\left(\frac{\Delta y_n}{\Delta x_n}\right) + \left(\frac{k_0 \Delta y_n}{2}\right)^2 \cdot \left(\frac{\pi}{2} - \arctan\left(\frac{\Delta y_n}{\Delta x_n}\right) \right) \right\} + \frac{ik_0^2 \Delta x_n \Delta y_n}{4} (\epsilon(x_n, y_n) - 1) \cdot \left\{ -A^i_{nn} + \beta \int_0^\infty e^{-\beta\nu} A^c_{nn}\, d\nu \right\}, \quad (33)$$

$$z_{2nn} = z_{3nn} = 0 \quad (34)$$

$$z_{4nn} = -1 - \frac{1}{\pi}(\epsilon(x_n, y_n) - 1) \left\{ \frac{k_0^2 \Delta x_n \Delta y_n}{4} \cdot \left[\ln\left(\frac{k_0}{4} \sqrt{\Delta x_n^2 + \Delta y_n^2} \right) + \gamma - \frac{i\pi}{2} - \frac{3}{2} \right] + 2\left(\frac{\pi}{2} - \arctan\left(\frac{\Delta y_n}{\Delta x_n}\right) \right) + \left(\frac{k_0 \Delta x_n}{2}\right)^2 \arctan\left(\frac{\Delta y_n}{\Delta x_n}\right) \right) \right\} + \frac{ik_0^2 \Delta x_n \Delta y_n}{4} (\epsilon(x_n, y_n) - 1) \cdot \left\{ C^i_{nn} - \beta \int_0^\infty e^{-\beta\nu} C^c_{nn}\, d\nu \right\}. \quad (35)$$

Upon comparing (13) and (15) the expressions for the elements of the impedance matrix for the impedance surface can be obtained by doubling the integral expressions, and replacing β by β' in (29)–(35).

The distance function in the integrand of all the integrals in the elements of the impedance matrix assumes a very small number when the observation and source points are both close to the surface of the resistive sheet. Since the singularity of the integrands in this case are much higher than the E polarization case, analytical evaluation of the integrals around the point ν_0 is even more critical. Fig. 4 shows the variation of the integrand as a function of ν for some typical values of source and observation points, and also compares the integrand with its approximation. It should be noted here that the phase of the integrand varies very rapidly around ν_0 resulting in a faster variation of the integrand than what is shown in Fig. 4. If the integral in (29) around the $\Delta\nu$ neighborhood of ν_0 is denoted by S_1 then

$$S_1 = e^{-\beta\nu_0} \left\{ H_0^{(1)}(k_0 r_0)(y_m + y_n + i\nu_0)^2 - \left[\left(\frac{i}{2\pi} - \frac{i\gamma}{\pi} - \frac{1}{2} \right) - \frac{i}{\pi} \ln\frac{k_0 r_0}{2} \right] \cdot \left[(x_m - x_n)^2 - (y_m + y_n + i\nu_0)^2 \right] \right\} I_2 - e^{-\beta\nu_0} \frac{2i}{\pi k_0^2} \left[(x_m - x_n)^2 - (y_m + y_n + i\nu_0)^2 \right] I_3$$

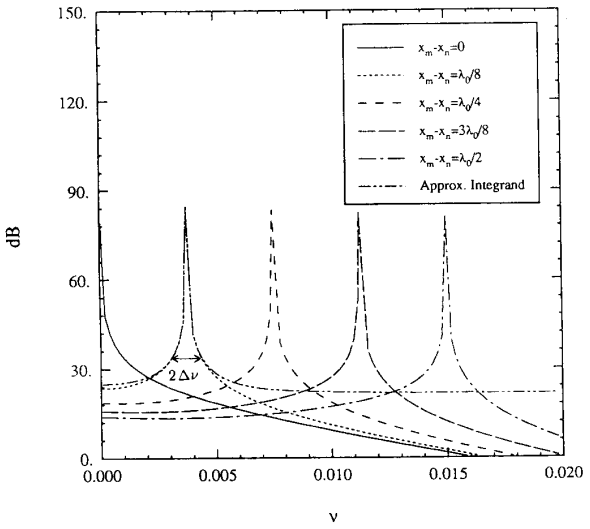

Fig. 4. The absolute value of the integrand function in (38) and its approximation for $R = 0.18 + i0.37$ at 10 GHz, $y_m + y_n = 6 \times 10^{-5}\ \lambda_0$, and five values of $x_m - x_n$.

where

$$I_2 = \frac{1}{2(x_m - x_n)} \ln \frac{r_0^2 + \Delta\nu^2 + 2(x_m - x_n)\,\Delta\nu}{r_0^2 + \Delta\nu^2 - 2(x_m - x_n)\,\Delta\nu},$$

$$I_3 = \frac{\Delta\nu}{(x_m - x_n)^2} \cdot \frac{r_0^2 - \Delta\nu^2 - 2(y_m + y_n + i\nu_0)^2}{(r_0^2 - \Delta\nu^2)^2 + 4\,\Delta\nu^2 (y_m + y_n + i\,\Delta\nu_0)^2} + \frac{1}{4(x_m - x_n)^3} \ln \frac{r_0^2 + \Delta\nu^2 + 2(x_m - x_n)\,\Delta\nu}{r_0^2 + \Delta\nu^2 - 2(x_m - x_n)\,\Delta\nu}.$$

In evaluation of the diagonal elements, we set $x_m = x_n$, which leads to $\nu_0 = 0$ and the integral in (33) is approximated by

$$S_1' = \frac{i2}{\pi k_0^2} I_3' + \frac{i}{\pi} I_2' + \left(\frac{i}{2\pi} + \frac{i\gamma}{\pi} - \frac{1}{2}\right)\Delta\nu,$$

where

$$I_2' = -i\left[(y_m + y_n) \ln \frac{y_m + y_n + i\,\Delta\nu}{y_m + y_n} + i\,\Delta\nu \ln \frac{k_0(y_m + y_n + i\,\Delta\nu)}{2} - i\,\Delta\nu\right]$$

$$I_3' = \frac{\Delta\nu}{(y_m + y_n)(y_m + y_n + i\,\Delta\nu)}.$$

To extract the contribution of the integrand in (30) around ν_0 we use similar approximations as in (29). If this integral is denoted by S_2, then

$$S_2 = e^{-\beta\nu_0}(x_m - x_n)(y_m + y_n + i\nu_0) \cdot \left\{\left[H_0^{(1)}(k_0 r_0) + \left(\frac{i}{\pi} - \frac{i2\gamma}{\pi} - 1\right) - \frac{i2}{\pi} \ln \frac{k_0 r_0}{2}\right] I_2 + \frac{4i}{\pi k_0^2} I_3\right\}.$$

The integral in (31) around the point ν_0 is approximated by S_3 where $S_3 = S_2$, and similarly for the integral in (32) if S_4 represents the integral around ν_0 then

$$S_4 = e^{-\beta\nu_0}\left\{H_0^{(1)}(k_0 r_0)(x_m - x_n)^2 + \left[\left(\frac{i}{2\pi} - \frac{i\gamma}{\pi} - \frac{1}{2}\right) - \frac{i}{\pi} \ln \frac{k_0 r_0}{2}\right] \cdot \left[(x_m - x_n)^2 - (y_m + y_n + i\nu_0)^2\right]\right\} I_2 + e^{-\beta\nu_0} \frac{2i}{\pi k_0^2}\left[(x_m - x_n)^2 - (y_m + y_n + i\nu_0)^2\right] I_3.$$

When $x_m = x_n$, then $\nu_0 = 0$ and this integral is represented by

$$S_4' = -\frac{i2}{\pi k_0^2} I_3' + \frac{i}{\pi} I_2' - \left(\frac{i}{2\pi} - \frac{i\gamma}{\pi} - \frac{1}{2}\right)\Delta\nu.$$

Once the system of linear equations for the polarization current has been solved the scattered field from the dielectric structure at any point in the upper half-space can be obtained by means of (17) for both E- and H-polarization cases.

V. Numerical Results

In this section the results based on the numerical solution are presented. As a verification of the numerical code we first compare the numerical solution of scattering echo width of a dielectric hump over a resistive sheet with a perturbation solution of the problem [16]. Consider a homogeneous dielectric hump with dielectric constant $\epsilon = 36 + i17$ over a resistive sheet with resistivity $R = 0.18 + i0.37$. Suppose the functional form of the hump is given by

$$y = \frac{w^2}{x^2 + w^2}\Delta$$

and that the hump is illuminated by a plane wave at 10 GHz ($\lambda_0 = 3$ cm). Figs. 5–8 show the bistatic echo width and the phase of the far-field amplitude of the hump for $\Delta = 3\lambda_0/1000$, $w = \lambda_0/15$, and $w = \lambda_0/25$ at incidence angles $\phi_0 = 0°$ and $\phi_0 = 45°$ for both polarizations. In each figure the results based on the perturbation technique are compared with the numerical results. The agreement is very good in spite of the fact that the perturbation solution is only a first order one. For thicker dielectric humps (larger Δ) the perturbation technique cannot be used and the moment method is the only available method of solution.

With confidence in the numerical code we now consider

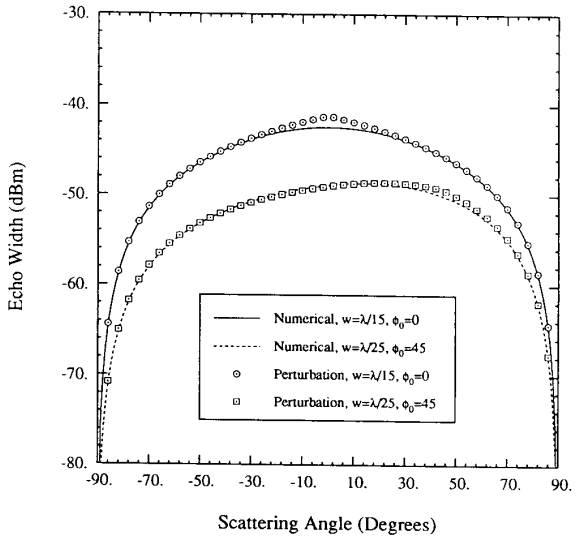

Fig. 5. Bistatic echo width of a dielectric hump with $\epsilon = 36 + i17$, and $\Delta = 3\lambda_0/1000$ over a resistive sheet with $R = 0.18 + i0.37$ at $f = 10$ GHz for E-polarization.

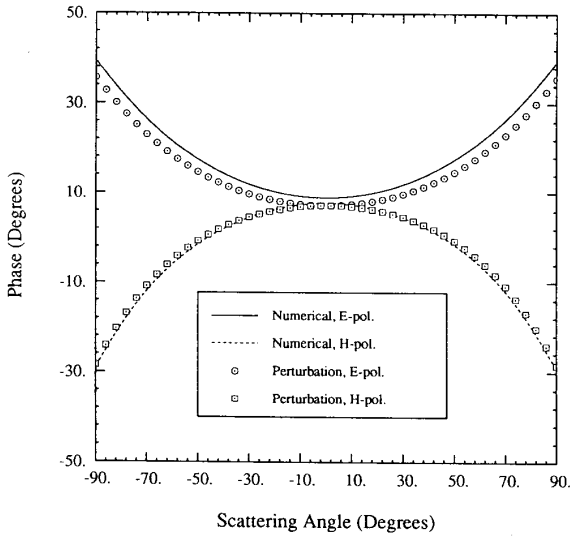

Fig. 7. Phase of far-field amplitude of a dielectric hump with $\epsilon = 36 + i17$, and $\Delta = 3\lambda_0/1000$ over a resistive sheet with $R = 0.18 + i0.37$ at $f = 10$ GHz and $\phi_0 = 0$ for E- and H-polarization.

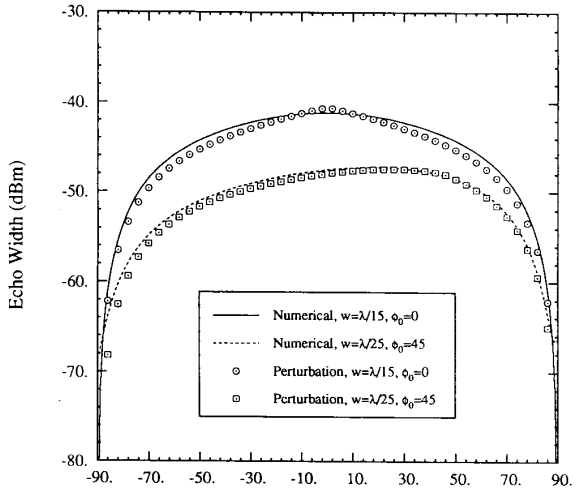

Fig. 6. Bistatic echo width of a dielectric hump with $\epsilon = 36 + i17$, and $\Delta = 3\lambda_0/1000$ over a resistive sheet with $R = 0.18 + i0.37$ at $f = 10$ GHz for H-polarization.

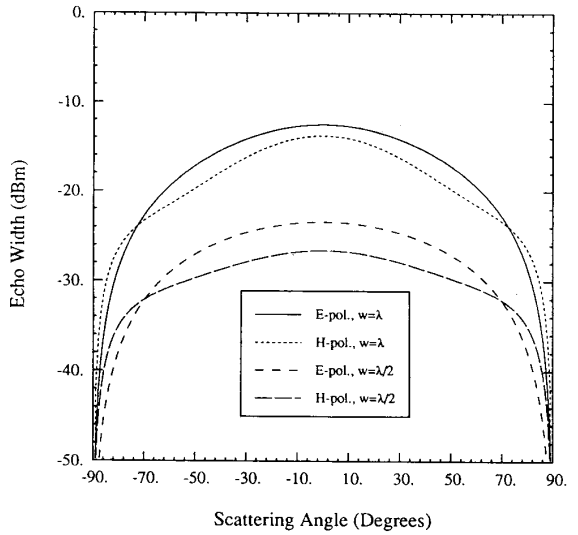

Fig. 8. Bistatic echo width of triangular humps with $\epsilon = 3 + i1$, over an impedance surface with $\eta = 0.21 - i0.04$ at $f = 10$ GHz for E- and H-polarization.

several examples with impedance surfaces. In all of the following examples the impedance of the surface is taken to be $\eta = 0.21 - i.04$ and the dielectric hump is assumed to be an isosceles triangle with base w and altitude $w/4$. The triangular humps are also considered to be homogeneous with $\epsilon = 3 + i1$ placed over the impedance surface. Figs. 8 and 9, respectively, show the bistatic echo width and phase of the far-field amplitude for two different sizes of triangular humps at normal incidence ($\phi_0 = 0°$) and $\lambda = 3$ cm. The angular dependency of the backscattering echo width of the same humps is shown in Fig. 10.

VI. Conclusion

An efficient numerical technique has been developed to compute the scattering behavior of inhomogeneous dielectric cylinders of arbitrary cross section above impedance surfaces and resistive sheets. The efficiency of this method is accomplished by deriving new expressions for the Green's function of the problem. Using an appropriate integral transformation the ordinary integral representation of the Green's function containing a highly oscillatory integrand was transformed into a new integral form that is rapidly convergent. Useful asymptotic expressions of the Green's function were also derived. Analytical treatment for singular behavior of Green's

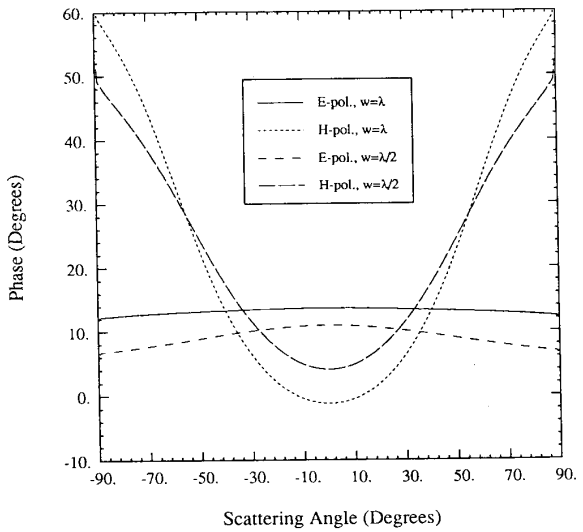

Fig. 9. Phase of far-field amplitude of triangular humps with $\epsilon = 3 + i1$, over an impedance surface with $\eta = 0.21 - i0.04$ at $f = 10$ GHz and $\phi_0 = 0$ for E- and H-polarization.

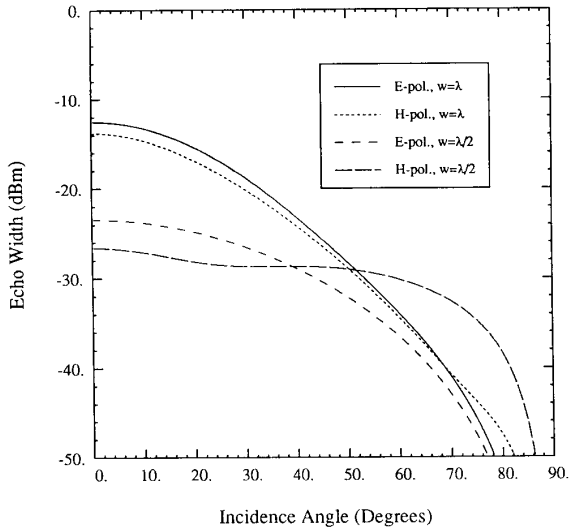

Fig. 10. Backscattering echo width of triangular humps with $\epsilon = 3 + i1$, over an impedance surface with $\eta = 0.21 - i0.04$ at $f = 10$ GHz for E- and H-polarization.

function when both the source and the observation points are close to the surface is given.

Several numerical examples are presented for resistive sheet and impedance surface problems. The accuracy of the numerical code is checked by comparing the numerical solution of scattering from a very thin dielectric hump above a resistive sheet with a perturbation method. Excellent agreement is obtained in all test cases.

Appendix

The following functions are defined to simplify the expressions for the elements of the impedance matrix in the H-polarization case

$$A^q_{mn} = H_0^{(1)}(k_0 r^q_{mn}) \sin^2\theta^q_{mn} + \frac{H_1^{(1)}(k_0 r^q_{mn})}{(k_0 r^q_{mn})} \cdot (2\cos^2\theta^q_{mn} - 1) + \frac{(\Delta x_n)^2}{24}\left(\frac{\partial^2}{\partial x^2} + k_0^2\right) U^q_{mn} + \frac{(\Delta y_n)^2}{24}\left(\frac{\partial^2}{\partial x^2} + k_0^2\right) V^q_{mn}$$

$$B^q_{mn} = -H_0^{(1)}(k_0 r^q_{mn}) + \frac{2H_1^{(1)}(k_0 r^q_{mn})}{(k_0 r^q_{mn})} \cos\theta^q_{mn} \sin\theta^q_{mn} + \frac{(\Delta x_n)^2}{24}\frac{\partial^2}{\partial x\,\partial y} U^q_{mn} + \frac{(\Delta y_n)^2}{24}\frac{\partial^2}{\partial x\,\partial y} V^q_{mn}$$

$$C^q_{mn} = H_0^{(1)}(k_0 r^q_{mn}) \cos^2\theta^q_{mn} + \frac{H_1^{(1)}(k_0 r^q_{mn})}{(k_0 r^s_{mn})} \cdot (2\sin^2\theta^q_{mn} - 1) + \frac{(\Delta x_n)^2}{24}\left(\frac{\partial^2}{\partial y^2} + k_0^2\right) U^q_{mn} + \frac{(\Delta y_n)^2}{24}\left(\frac{\partial^2}{\partial y^2} + k_0^2\right) V^q_{mn}$$

where the derivatives of the functions defined by (24) and (25) are given by

$$\frac{\partial^2}{\partial x^2} U^q_{mn} = k_0^2 \Bigg\{ H_0^{(1)}(k_0 r^q_{mn}) \Bigg[\cos^2\theta^q_{mn}\left(\frac{1}{4}\cos^2\theta^q_{mn} + \frac{1}{8}\right) + \frac{2\sin^2\theta^q_{mn}}{(k_0 r^q_{mn})^2}(4\cos^2\theta^q_{mn} - 1)\Bigg] + H_1^{(1)}(k_0 r^q_{mn}) \Bigg[\frac{5}{k_0 r^q_{mn}} \cos^2\theta^q_{mn}\sin^2\theta^q_{mn} - \frac{4\sin^2\theta^q_{mn}}{(k_0 r^q_{mn})^3}(4\cos^2\theta^q_{mn} - 1)\Bigg] + H_2^{(1)}(k_0 r^q_{mn}) \Bigg[-\frac{1}{2}\cos^4\theta^q_{mn} + \frac{\sin^2\theta^q_{mn}}{(k_0 r^q_{mn})^2}(-10\cos^2\theta^q_{mn} + 1)\Bigg] + H_4^{(1)}(k_0 r^q_{mn}) \Bigg[\frac{1}{8}\cos^2\theta^q_{mn}(2\cos^2\theta^q_{mn} - 1)\Bigg] \Bigg\}$$

$$\frac{\partial^2}{\partial y^2} U^q_{mn} = k_0^2 \Bigg\{ H_0^{(1)}(k_0 r^q_{mn}) \Bigg[\sin^2\theta^q_{mn}\left(\frac{1}{4}\cos^2\theta^q_{mn} + \frac{1}{8}\right) + \frac{2\cos^2\theta^q_{mn}}{(k_0 r^q_{mn})^2}(1 - 4\sin^2\theta^q_{mn})\Bigg] + H_1^{(1)}(k_0 r^q_{mn}) \Bigg[-\frac{4}{k_0 r^q_{mn}} \cos^2\theta^q_{mn}\sin^2\theta^q_{mn}$$

$$+\frac{4\cos^2\theta_{mn}^q}{(k_0 r_{mn}^q)^3}(4\sin^2\theta_{mn}^q-1)\Bigg]$$
$$+H_2^{(1)}(k_0 r_{mn}^q)\Bigg[-\frac{1}{2}\sin^2\theta_{mn}^q\cos^2\theta_{mn}^q$$
$$+\frac{\cos^2\theta_{mn}^q}{(k_0 r_{mn}^q)^2}(10\sin^2\theta_{mn}^q-1)\Bigg]$$
$$+H_4^{(1)}(k_0 r_{mn}^q)\Bigg[\frac{1}{8}\sin^2\theta_{mn}^q(2\cos^2\theta_{mn}^q-1)\Bigg]\Bigg\}$$

$$\frac{\partial^2}{\partial x\,\partial y}U_{mn}^q = k_0^2\sin\theta_{mn}^q\cos\theta_{mn}^q$$
$$\cdot\Bigg\{H_0^{(1)}(k_0 r_{mn}^q)\Bigg[\frac{1}{4}\cos^2\theta_{mn}^q+\frac{1}{8}$$
$$+\frac{4}{(k_0 r_{mn}^q)^2}(2\sin^2\theta_{mn}^q-1)\Bigg]$$
$$+H_1^{(1)}(k_0 r_{mn}^q)\Bigg[\frac{1}{k_0 r_{mn}^q}(2-5\cos^2\theta_{mn}^q)$$
$$+\frac{8}{(k_0 r_{mn}^q)^3}(2\cos^2\theta_{mn}^q-1)\Bigg]$$
$$+H_2^{(1)}(k_0 r_{mn}^q)\Bigg[-\frac{1}{2}\cos^2\theta_{mn}^q$$
$$+\frac{5}{(k_0 r_{mn}^q)^2}(2\cos^2\theta_{mn}^q-1)\Bigg]$$
$$+H_4^{(1)}(k_0 r_{mn}^q)\Bigg[\frac{1}{8}(2\cos^2\theta_{mn}^q-1)\Bigg]\Bigg\}$$

$$\frac{\partial^2}{\partial x^2}V_{mn}^q = k_0^2\Bigg\{H_0^{(1)}(k_0 r_{mn}^q)\Bigg[\cos^2\theta_{mn}^q\Big(\frac{1}{4}\sin^2\theta_{mn}^q+\frac{1}{8}\Big)$$
$$+\frac{2\sin^2\theta_{mn}^q}{(k_0 r_{mn}^q)^2}(1-4\cos^2\theta_{mn}^q)\Bigg]$$
$$+H_1^{(1)}(k_0 r_{mn}^q)\Bigg[\frac{\sin^2\theta_{mn}^q}{k_0 r_{mn}^q}(-5\cos^2\theta_{mn}^q+1)$$
$$+\frac{4\sin^2\theta_{mn}^q}{(k_0 r_{mn}^q)^3}(4\cos^2\theta_{mn}^q-1)\Bigg]$$
$$+H_2^{(1)}(k_0 r_{mn}^q)\Bigg[-\frac{1}{2}\sin^2\theta_{mn}^q\cos^2\theta_{mn}^q$$
$$+\frac{\sin^2\theta_{mn}^q}{(k_0 r_{mn}^q)^2}(10\cos^2\theta_{mn}^q-1)\Bigg]$$
$$+H_4^{(1)}(k_0 r_{mn}^q)\Bigg[\frac{1}{8}\cos^2\theta_{mn}^q(2\sin^2\theta_{mn}^q-1)\Bigg]\Bigg\}$$

$$\frac{\partial^2}{\partial y^2}V_{mn}^q = k_0^2\Bigg\{H_0^{(1)}(k_0 r_{mn}^q)\Bigg[\sin^2\theta_{mn}^q\Big(\frac{1}{4}\sin^2\theta_{mn}^q+\frac{1}{8}\Big)$$
$$+\frac{2\cos^2\theta_{mn}^q}{(k_0 r_{mn}^q)^2}(4\sin^2\theta_{mn}^q-1)\Bigg]$$
$$+H_1^{(1)}(k_0 r_{mn}^q)\Bigg[\frac{5}{k_0 r_{mn}^q}\sin^2\theta_{mn}^q\cos^2\theta_{mn}^q$$
$$-\frac{4\cos^2\theta_{mn}^q}{(k_0 r_{mn}^q)^3}(4\sin^2\theta_{mn}^q-1)\Bigg]$$
$$+H_2^{(1)}(k_0 r_{mn}^q)\Bigg[-\frac{1}{2}\sin^4\theta_{mn}^q$$
$$-\frac{\cos^2\theta_{mn}^q}{(k_0 r_{mn}^q)^2}(10\sin^2\theta_{mn}^q-1)\Bigg]$$
$$+H_4^{(1)}(k_0 r_{mn}^q)\Bigg[\frac{1}{8}\sin^2\theta_{mn}^q(2\sin^2\theta_{mn}^q-1)\Bigg]\Bigg\}$$

$$\frac{\partial^2}{\partial x\,\partial y}V_{mn}^q = k_0^2\sin\theta_{mn}^q\cos\theta_{mn}^q$$
$$\cdot\Bigg\{H_0^{(1)}(k_0 r_{mn}^q)\Bigg[\frac{1}{4}\sin^2\theta_{mn}^q+\frac{1}{8}$$
$$+\frac{4}{(k_0 r_{mn}^q)^2}(2\cos^2\theta_{mn}^q-1)\Bigg]$$
$$+H_1^{(1)}(k_0 r_{mn}^q)\Bigg[\frac{1}{k_0 r_{mn}^q}(2-5\sin^2\theta_{mn}^q)$$
$$+\frac{8}{(k_0 r_{mn}^q)^3}(2\sin^2\theta_{mn}^q-1)\Bigg]$$
$$+H_2^{(1)}(k_0 r_{mn}^q)\Bigg[-\frac{1}{2}\sin^2\theta_{mn}^q$$
$$+\frac{5}{(k_0 r_{mn}^q)^2}(2\sin^2\theta_{mn}^q-1)\Bigg]$$
$$+H_4^{(1)}(k_0 r_{mn}^q)\Bigg[\frac{1}{8}(2\sin^2\theta_{mn}^q-1)\Bigg]\Bigg\}$$

References

[1] F. T. Ulaby, R. K. Moore, and A. K. Fung, *Microwave Remote Sensing: Active and Passive, Vol. II—Radar Remote Sensing and Surface Scattering and Emission Theory*. Norwood, MA: Artech House, 1986.

[2] K. Sarabandi, Y. Oh, F. T. Ulaby, "Polarimetric radar measurement of bare soil surfaces at microwave frequencies," in *Proc. IEEE Geosci. Remote Sensing Symp.*, Espoo, June 1991, pp. 387–390.

[3] J. A. Stratton, *Electromagnetic Theory*. New York: McGraw-Hill, 1941.

[4] Y. Rahmat-Samii, R. Mittra, and P. Parhami, "Evaluation of Sommerfeld integrals for lossy half-space problems," *Electromagn.*, vol. 1, no. 1, pp. 1–28, 1981.

[5] P. Parhami, Y. Rahmat-Samii, and R. Mittra, "An efficient approach for evaluating Sommerfeld integrals encountered in the problem of a current element radiating over lossy ground," *IEEE Trans. Antennas Propagat.*, vol. AP-28, pp. 100–104, 1980.

[6] J. S. Izadian, L. Peters, and J. H. Richmond, "Computation of scattering from penetrable cylinders with improved numerical efficiency," *IEEE Trans. Geosci. Remote Sensing*, vol. GE-22, pp. 52–61, 1984.

[7] J. R. Parry and S. H. Ward, "Electromagnetic scattering from cylinders of arbitrary cross section in a conducting half-space," *Geophys.*, vol. 36, no. 1, pp. 67-100, 1971.
[8] I. V. Lindell and E. Alanen, "Exact image theory for the Sommerfeld half-space problem, Part III: General formulation," *IEEE Trans. Antennas Propagat.*, vol. AP-32, pp. 1027-1032, 1984.
[9] I. V. Lindell, A. H. Sihvola, K. O. Muinonen, and P. W. Barber, "Scattering by a small object close to an interface, I: Exact image theory formulation," *JOSA*, no. A 8, pp. 472-476, 1991.
[10] I. V. Lindell, K. I. Nikoskinen, E. Alanen, A. T. Hujanen, "Scalar Green's function method for microstrip antenna analysis based on the exact image theory," *Ann. Telecommun.*, vol. 44, pp. 533-542, 1989.
[11] L. B. Felson and N. Marcuvitz, *Radiation and Scattering of Waves*. Englewood Cliffs, NJ: Prentice-Hall, 1973.
[12] G. Tyras, *Radiation and Propagation of Electromagnetic Waves*. New York: Academic, 1965.
[13] T. B. A. Senior, K. Sarabandi, and F. T. Ulaby, "Measuring and modeling the backscattering cross section of a leaf," *Radio Sci.*, vol. 22, pp. 1109-1116, 1987.
[14] J. H. Richmond, "Scattering by a dielectric cylinder of arbitrary cross section shape," *IEEE Trans. Antennas Propagat.*, vol. AP-13, pp. 334-341, May 1965.
[15] D. C. Handscomb, *Method of Numerical Approximations*. New York: Pergamon, 1966.
[16] K. Sarabandi, "Scattering from variable resistive and impedance sheets," *J. Electromagn. Waves Appl.*, vol. 4, no. 9, pp. 865-891, 1990.

Kamal Sarabandi, for a photograph and biography please see page 1110 of the July 1990 issue of this TRANSACTIONS.